International Journal of Nanomedicine

Dovepress
open access to scientific and medical research

Open Access Full Text Article

ORIGINAL RESEARCH

Engineering of Neutrophil Membrane Camouflaging Nanoparticles Realizes Targeted Drug Delivery for Amplified Antitumor Therapy

This article was published in the following Dove Press journal:
International Journal of Nanomedicine

Jingshuai Wang[1,*]
Xuemin Gu[1,*]
Yiqin Ouyang[1]
Lei Chu[1]
Mengjiao Xu[1]
Kun Wang[2]
Xiaowen Tong[1]

[1]Obstetrics and Gynecology Department, Tongji Hospital of Tongji University, Shanghai, People's Republic of China; [2]Cancer Center, Shanghai East Hospital of Tongji University, Shanghai, People's Republic of China

*These authors contributed equally to this work

Purpose: Although the neutrophil membrane (NM)-based nanoparticulate delivery system has exhibited rapid advances in tumor targeting stemmed from the inherited instinct, the antitumor effect requires further improvement due to inefficient cellular internalization in the absence of specific interactions between NM-coated nanoparticles and tumor cells.

Methods: Herein, we fabricated drug-paclitaxel loaded NM camouflaging nanoparticles (TNM-PN) modified with tumor necrosis factor-related apoptosis-inducing ligand (TRAIL), favorable for the cellular internalization.

Results: The results showed that TNM-PN exerted a significant cytotoxicity to tumor cells by TRAIL-mediated endocytosis and strong adhesion to inflamed endothelial cells in vitro. Due to TRAIL modification as well as the adhesive interactions between neutrophil and inflamed tumor vascular endothelial cells, tumors in TNM-PN group exhibited almost 2-fold higher fluorescence intensities than that of NM camouflaging nanoparticles and 3-fold higher than that of bare nanoparticles, respectively. Significant tumor inhibition and survival rates of mice were achieved in TNM-PN group as a consequence of prolonged blood circulations to 48 h and preferential tumor accumulations, which was ascribed to targeting adhesion originated from NM to immune evasion and subsequent excellent cellular internalization.

Conclusion: The research unveiled a novel strategy of amplifying cellular internalization based on NM coating nanotechnology to boost antitumor efficacy.

Keywords: neutrophil membrane camouflaging, nanoparticulate delivery, tumor targeting, cellular internalization, antitumor therapy

Introduction

In the past decades, nanoparticular drug delivery systems have shown considerable advances for cancer therapy,[1] while there exist many unsettled obstacles, such as insufficient tumor-targeting accumulation and subsequent cellular internalization,[2–4] to limit their clinical applications. Among the implements for extending the applications, biomimetic nanotechnology, which may help bypass potential bottlenecks and has attracted substantial attention in recent years, provides an inspiring vision.[5,6] Biomimetic nanoparticles disguised with cell membranes derived from original cells can usually escape immune surveillance to prolong the circulating half-life.[6–8] Simultaneously, due to the inherited instinct in terms of circulation and targetability, nanoparticles with the cell membrane cloak are more likely to accumulate in tumors.[9–12] In respect of employing cell membranes for tumor-targeting, neutrophil membrane (NM) has been an ideal alternative mostly resulting from the

Correspondence: Kun Wang
Jimo Road 150, Pudong New District, Shanghai, People's Republic of China
Email 001wangkun@tongji.edu.cn

Xiaowen Tong
Xincun Road 389, Putuo District, Shanghai, People's Republic of China
Email Xiaowen_tong@hotmail.com

submit your manuscript | www.dovepress.com
DovePress
http://doi.org/10.2147/IJN.S288636

interaction between the neutrophil and inflamed endothelium of tumor tissue.[13,14] It has been evidenced that the specific mechanism of targeting depends on the active neutrophils' adhesion naturally to intercellular adhesion molecule-1 (ICAM-1) overexpressed in tumor-associated vasculature.[15] Consequently, NM-coated nanoparticles are prone to target the tumor, which has been utilized for antitumor applications.[16]

However, as it stands, biomimetic nanoparticles loading cargoes have to overcome an additional barrier of unmet cellular internalization after releasing drugs into tumor tissue gaps to exert therapeutic function. In the current stage, neutrophil coated nanoparticles face the added challenge of indistinct interactions between NM and solid tumor cells.[16,17] To circumvent the limitation, there is an urgent need to remodel NM-coated nanoparticle with potent internalization capacity for better targeting therapy efficiently.[18] To the best of our knowledge, very little research has focused on the investigation of how to help drug-loaded biomimetic nanoparticle realize internalization by tumor cells.

As for mediating the cellular internalization, many functional groups, such as cancer-specific targeting ligands (eg, antibodies, small molecules, and peptides), have been extensively explored to potentiate tumor targeting.[18] Of note, the ligands on the nanoparticles are probably endowed with abilities of recognition and adherence to tumor cells by corresponding receptors and trigger receptor-mediated endocytosis. Tumor necrosis factor-related apoptosis-inducing ligand (TRAIL), an immune cytokine secreted by immune cells, is capable of bounding to death receptors 4 and 5 (DR4 and DR5) overexpressed on the surface of various tumor cells to trigger caspases or mitochondrial-dependent death without toxicity in vivo.[19–21] TRAIL also plays a pivotal role as a targeting ligand mediating the cellular internalization by directly binding with its receptor.[22,23] Thus, TRAIL-based therapies have been applied in clinical trials and have shown minimal adverse effects for patients with several kinds of tumors, but little therapeutic efficacy as monotherapy due to poor circulation half-life, inefficient tumor targeting, and TRAIL resistance.[21,24,25] Nanoparticulate delivery systems hold promise for eliminating the TRAIL delivery barriers in vivo to facilitate tumor ablation.[21,26–28] For instance, TRAIL and transferrin were modified onto the surface of human serum albumin nanoparticles (NPs) containing doxorubicin (Dox) to induce various types of tumor cells apoptosis.[29] Besides, Dox-loaded liposomes, coated with both TRAIL and the cell-penetrating peptide R8H3, were engineered with hyaluronic acid gels, which had also been designed for tumor therapy.[30] Hence, the alternative for optimizing TRAIL is compelling for phagocytosis of biomimetic nanoparticles.

Based on this rationale, a novel NM-based biomimetic nanoparticle delivery system was developed, achieving specific internalization into tumor cells and robust antitumor effect by virtue of the engineering of TRAIL. In this research, FDA-approved PLGA was employed as the core, which was preloaded with the chemotherapeutic drug-paclitaxel (PTX).[28,31] After camouflaged with NM, TRAIL was introduced into the hybrid system to bind to tumor cells for the promotion of cellular internalization, which further induced apoptosis (Figure 1). Particularly, the adherence to the inflamed endothelial cells by the neutrophil membrane boosted the accumulation of biomimetic nanoparticles at the tumor site, as well as a significant inhibition of tumor growth. The highlight in this work was the prominence of mediating cellular internalization to achieve efficient tumor-targeting, which was different from the prevailing designs on functional cell membrane camouflaged nanoparticles.

Materials and Methods

Materials

Acetonitrile, dimethyl sulfoxide (DMSO) and paclitaxel were purchased from Aladdin Chemistry Co. Ltd. 1, 1′-dioctadecyl-3, 3, 3′, 3′-tetramethylindodicarbocyanine, 4-chlorobenzenesulfonate salt (DiD) dye, were provided by Invitrogen (USA). Tumor necrosis factor-related apoptosis-inducing ligand (TRAIL) was provided by Genscript Biotech (China). Recombinant human TNF-α, 4, 6-diamidino-2-phenylindole (DAPI), CCK-8 KIT, paraformaldehyde solution, SDS-PAGE gel, annexin V-fluorescein isothiocyanate (Annexin V-FITC)/propidium iodide (PI) apoptosis and necrosis detection kit, trypsin and penicillin-streptomycin were purchased from Beyotime Biotechnology Co. Ltd. (China). Roswell Park Memorial Institute (RPMI) 1640 medium, Dulbecco's modified Eagle's medium (DMEM) and fetal bovine serum (FBS) were obtained from Gibco Life Technologies (USA). 96-well plates, 6-well plates, confocal laser dishes and cell culture dishes were provided by Corning. All other reagents were used as received directly. FITC-CD11b antibody and PE/Cy7-Ly-6G/Ly-6C antibody were purchased from BD Biosciences. Antibodies used in Western Blot

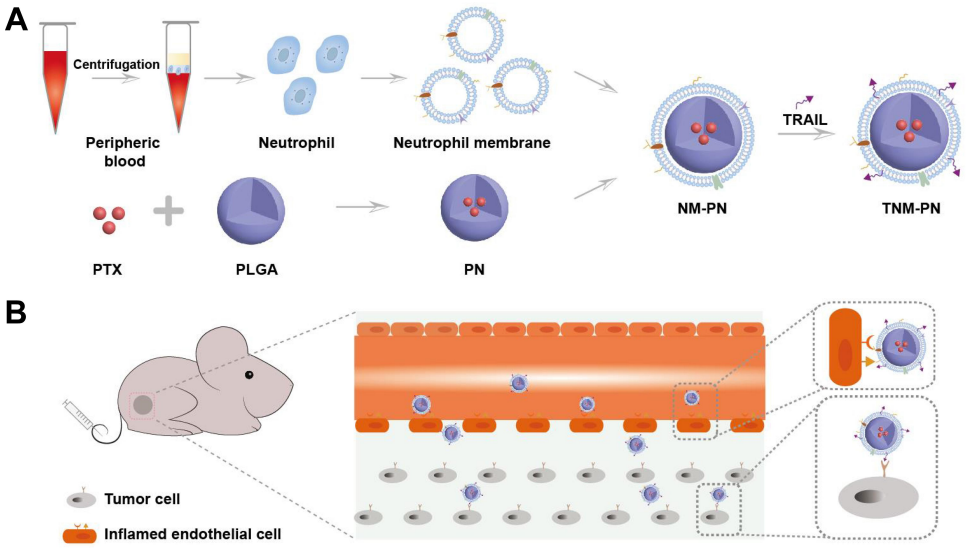

Figure 1 Schematic illustration of the structure and assembly of TNM-PN and in vivo antitumor therapy mechanism. (**A**) The neutrophil membranes were isolated to coat PLGA-PTX nanoparticles to form NM-PN, which subsequently were modified with TRAIL to achieve TNM-PN. (**B**) Schematic illustration of in vivo antitumor therapy of TNM-PN through the adhesion between inflamed tumor vascular endothelial cells and neutrophil membranes onto the nanoparticles, and subsequent active targeting to tumor cells as a consequence of the interaction of TRAIL with its receptors.

were purchased from Abcam China. SKOV3 cells, RAW264.7 cells and human umbilical vein endothelial cells (HUVECs) were purchased from the Chinese Academy of Sciences Cell Bank (Shanghai, China). Female Balb/c nude mice were purchased from Shanghai Slack laboratory animal Co., Ltd. All the animal procedures were performed in accordance with the Guidelines for Care and Use of Laboratory Animals of Tongji University (Shanghai, China) and approved by the Animal Ethics Committee of Tongji University, School of Medicine (Shanghai, China).

Isolation of Neutrophil and NM

Neutrophils were harvested by sucrose gradient centrifugation according to the previous report.[32] Briefly, 3–4 weeks old mice were euthanized to isolate neutrophils from peripheral blood in advance, followed by suspending in PBS and centrifuging to collect purified neutrophils. Afterwards, 2 mL separation mixed solution containing 55, 65, and 78% (v:v) Percoll in PBS was added into the tube with collected neutrophils. The mixed solution was centrifuged for 25 min at 2000 rpm. Subsequently, neutrophils were harvested at the interface of the 65 and 78% fractions. Before analyzing the purity by FCM, the neutrophils were doubly stained with PE/Cy7-Ly-6G/Ly-6C and FITC-CD11b.

To isolate the NM, neutrophils were firstly treated with hypotonic lysing buffer (PBS). Before centrifugation to get the cell pellet, the cell suspension with buffer was further homogenized with the speed of 12,000 rpm. Afterwards, the pellet and the supernatant were centrifuged again at 120 000 g for 60 min at 4 °C. The cell membranes in the bottom of the tube were collected, which were also washed with PBS twice. The purified cell membrane was freeze-dried and stored at 4 °C.

Synthesis of PN, NM-PN and TPN-NM

PLGA nanoparticles were synthesized according to the procedures: PLGA (4 mg) was resolved in acetonitrile (1 mL), which was added to water (3 mL) dropwise. The organic phase in the mixture was removed under a vacuum aspirator which can evaporate acetonitrile entirely. During this process, PTX could be encapsulated to produce PTX-loading PLGA nanoparticles (PN). To generate NM-coated PN (NM-PN), cell membranes were pre-treated by sonication and extruded by 400 nm and 100 nm carbonate membrane before mixing with PN. The mixture was following treated by the extrusion with 100 nm carbonate membrane and further sonication to homodisperse. TRAIL modified NM-PN (TNM-PN) was synthesized by the crosslinker reagents of sulfosuccinimidyl-4-(N-maleimidomethyl) cyclohexane-1-carboxylate (Sulfo-SMCC) reported in the previous literature.[8]

In vitro Evaluations of Stability and Cumulative Release

TNM-PN and NM-PN were suspended in DMEM containing 10% FBS. At an interval of 24 hours, the sizes of

nanoparticles were monitored by Dynamic light scattering (DLS).

In vitro cumulative release profile of PTX in TNM-PN and NM-PN was carried out. Briefly, the solutions of PN, NM-PN and TNM-PN was placed in the dialysis bags (MWCO of 10 kDa) immersed in 50 mL of PBS, followed by the continuous stirring in a water bath at 37 °C. At predetermined time intervals (0.5, 1, 2, 4, 8, 12, 24, 48, and 72 h), 5 mL aliquots were withdrawn from the dialysis solution to measure PTX. The amounts of released PTX were determined by High Performance Liquid Chromatography (HPLC). In total, 5 mL fresh PBS was added to remain the total volume of the dialysis solution constant after each sampling.

Cell Viability Evaluation

Ovarian cancer cell line-SKOV3 cells were seeded in a 96-well plate and incubated with RPMI 1640 medium at 37 °C, 5% CO_2, respectively. After the cell confluence reached around 70%-80%, then the medium was removed and replaced with fresh medium containing T-NM, NM-PN, TRAIL+NM-PN and TNM-PN for another 24 h incubation. The concentration of PTX varied from 0.5 to 10 μg mL^{-1} and TRAIL varied from 0.04 to 0.64 μg mL^{-1}, respectively. The cells were washed with PBS twice after co-incubation and 10 μL of the CCK-8 solution was added to each well and further incubated for 2 h. Cells without treatment were used as control. The absorbance was measured at 450 nm to calculate the viability using a microplate reader (Thermo Scientific, USA).

In vitro Tumor Cell Uptake Behavior

Fluorescent labeled TNM-PN and NM-PN were obtained by DiD dye loaded nanoparticles and dissolved in the medium. SKOV3 cells were cultivated in the laser confocal dishes to 80% −85% confluences. Then, the cells were washed by PBS twice and incubated with fluorescent-labeled TNM-PN and NM-PN for 4 h, respectively. The cells were rinsed with PBS twice, fixed with 4% paraformaldehyde for 5 min and rinsed three times with PBS. The cell nuclei were stained with DAPI for 5 min. The prepared samples were recorded to observe TNM-PN intracellular distributions by a confocal laser scanning microscope (CLSM).

To quantitatively evaluate the cellular uptake of TNM-PN and NM-PN, flow cytometry was employed to measure the fluorescence intensity of cells after the incubation at various time points. Briefly, cells were seeded in a 6-well plate to 70% confluence and then incubated with DiD-labeled TNM-PN and NM-PN for 4 h. After washing cells twice, the fluorescence intensity was determined.

Binding to Endothelial Cells

To determine the interaction between NM coating biomimetic nanoparticles and inflamed endothelium, the experiment of binding to endothelial cells in vitro was performed. Briefly, human umbilical vein endothelial cells (HUVECs) were planted in laser confocal dishes at a density of 2×10^5 cells/well in 2 mL of fresh medium. The cytokine of TNF-α was added into the medium to stimulate inflammatory responses for 6 h to 70% confluence. DiD-labeled TNM-PN was added into the dishes and further incubated for another 4 h. Cells without stimulation with TNF-α were incubated with DiD-labeled TNM-PN as a negative control. After that, the cells were washed and fixed with 4% paraformaldehyde, followed by staining with DAPI. The binding behavior was visualized and recorded by CLSM. To quantitatively analyze the binding profile in vitro, HUVECs were collected after incubation with DiD-labeled TNM-PN to measure the mean fluorescence intensity by flow cytometry.

In vitro Uptake by Macrophage

RAW264.7 cells were seeded in 6-well plates (1.5×10^6 cells/well) for 24 h. Then fresh medium containing samples (TNM-PN, NM-PN and PN preloaded with DiD) was added into 6-well plates to incubate for another 4 h. Subsequently, the cells were washed with PBS thrice, fixed with 4% paraformaldehyde solution, stained with DAPI, and finally observed by the CLSM. To quantitatively analyze the uptake of nanoparticles, RAW264.7 cells incubated with samples were harvested to determine mean florescence intensity by flow cytometry.

Pharmacokinetics in the Mice

To investigate the pharmacokinetics in the mice, TNM-PN, NM-PN and PN pre-labeled with DiD were injected intravenously into the mice. Then, the blood of the mice was collected at the predetermined time points (0.5, 1, 2, 4, 8, 12, 24, and 48 h). The blood samples were centrifuged at the speed of 800 rpm for 3 min to separate the serum, followed by determining the fluorescence intensity of biomimetic nanoparticles.

In vivo Investigation of Monocyte Uptake

TNM-PN, NM-PN and PN labeled with DiD were injected intravenously into the nude mice and the blood was

collected at 4 h post-injection. Red blood cell lysis buffer was added to remove erythrocytes, followed by collecting the remaining cells with centrifugation at 800 × g for 5 min. Afterwards, the cells were stained by CD16/CD32 antibody to block non-specific interactions for 15 min, followed by staining with FITC-anti-mouse CD11b for 30 min. The samples were then washed twice and re-suspended in a flow buffer. The monocyte uptake behavior was analyzed by flow cytometry.

In vivo Investigation of Tumor Targeting

The nude mice were inoculated with SKOV3 cells in the right flank to establish the tumor-bearing model. When the volume of the tumor arrived at around 100 mm^3, Ce6-encapsulated PN, NM-PN and TNM-PN were injected intravenously into the mice. At regular intervals (4, 12, 24, and 24 h), the mice were imaged by in vivo imaging system (CRI maestro). Following that, the mice were euthanized and tumors as well as major organs, including heart, liver, spleen, lung and kidney, were isolated to image directly. In the last stage, the fluorescence intensities of region-of-interests (ROI) were calculated by Living Image Software.

In vivo Investigation of Antitumor Therapy

The tumor-bearing models were established as mentioned above. When the tumor volume reached around 100 mm^3, five groups of the mouse (n=6) were intravenously injected with PN, NM-PN, TRAIL+NM-PN and TNM-PN every other day for 7 times, while PBS as the control. Tumor growth was measured at 2 days interval for 24 days using an electronic digital caliper. The volume of the subcutaneous tumor was estimated using the following formula: (short diameter) ^{2} × long diameter × 0.5. The weight of the mice was monitored to evaluate the side effects, and the survival rate was also recorded within 30 days. To further analyze the antitumor therapy outcome, the mice were euthanized to isolate tumors to image and weigh on the 17th day. Afterwards, H&E staining and Western blot assay of tumor tissues were preformed to observe the cell apoptosis.

Results and Discussions

Neutrophils were isolated from the peripheral blood and purified by density-gradient centrifugation according to the manufacturer′s instructions. The purity of $CD11b^+$ $Ly6G/Ly6C^+$ cells was quantified to be over 96% by FCM (Figure 2A, insert) and the morphologies of isolated cells were rounded with a diameter of 8–12 μm assessed by microscope (Figure 2A). PTX loaded PLGA nanoparticles (PN) were synthesized and the morphology was observed via Transmission Electron Microscope (TEM). Representative TEM images of PN showed well-dispersed, regular spherical nanoparticles with an average size of 55 nm (Figure 2B). After being coated with cell membranes and modified with TRAIL, TNM-PN exhibited a typical core-shell structure with an increased average diameter of around 70 nm (Figure 2C). The hydrated size distributions of PN, NM-PN and TNM-PN determined by dynamic light scattering (DLS) were consistent with TEM results (Figure 2D). The surface charges of TNM-PN and NM-PN were around −20 mV but PN with −33mV, indicating that cell membranes were successfully coated onto PN (Figure 2E). NM-PN modified with FITC labeled TRAIL exhibited typical absorbance peak of FITC, indicating that TRAIL was successfully decorated onto the surface of NM-PN (Figure 2F).

Following that, SDS-PAGE (sodium dodecyl sulfate-polyacrylamide gel electrophoresis) was performed to analyze the membrane protein components before and after the decoration. As shown in Figure 2G, no significant loss of membrane proteins was observed in neutrophils, NM and NM-PN groups during the process of cell membrane coating. It implied that the integrity of cell membranes onto nanoparticles was preserved to assure adhering to inflamed vascular endothelial cells effectively.

TNM-PN and NM-PN displayed considerable serum stability when cultured in DMEM containing 10% FBS (Figure 2H), which contributed to in vivo circulation. The release kinetics profiles of PTX in PN, NM-PN and TNM-PN were shown in Figure 2I. The results showed that no initial burst release was detected for PN, NM-PN and TNM-PN. The PTX was released in a sustained manner from PN, NM-PN and TNM-PN up to 120 h. There was an approximate 50% PTX releasing from TNM-PN and NM-PN, exhibiting a comparable level with that from PN, suggesting that PTX could be released despite the cell membrane camouflaging. Therefore, it can be concluded that PTX in TNM-PN exhibited a sustained release profile which would be in favor of cancer therapy.

The cytotoxicity of SKOV3 cells treated with biomimetic nanoparticles was assessed by CCK-8 kit according to the manufacturer′s instructions. As shown in Figure 3A, the TNM-PN group displayed the most significant toxic effects

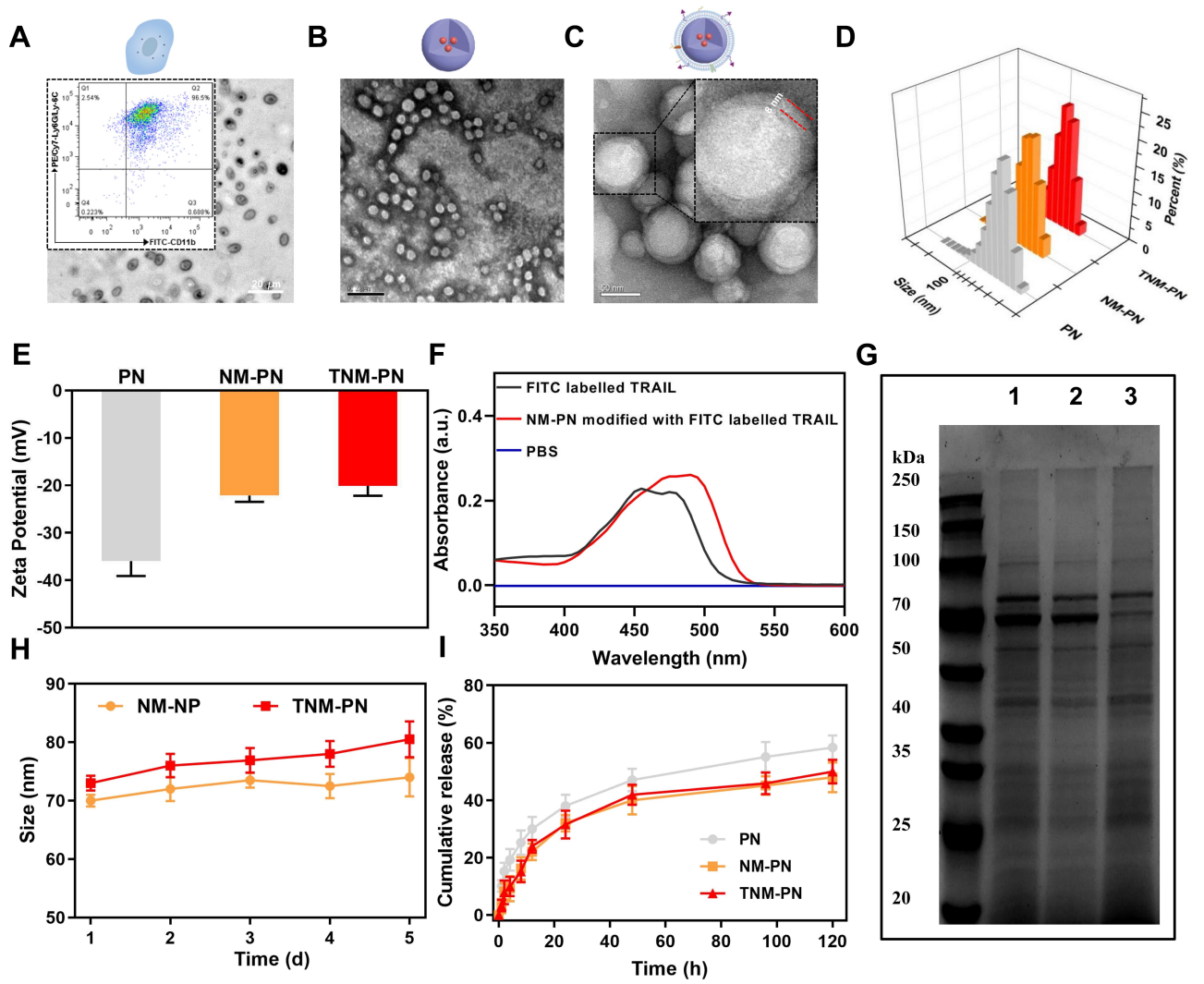

Figure 2 Characterizations of the physicochemical properties of biomimetic nanoparticles. (**A**) The purity (insert) and morphology of isolated neutrophils determined by FCM and microscope. Representative morphology imagines of (**B**) PN (scale bar= 200 nm) and (**C**) TNM-PN observed by TEM (scale bar= 50 nm). (**D**) Hydrodynamic size distributions and (**E**) zeta potentials of PN, NM-PN and TNM-PN were analyzed by DLS, respectively. (**F**) UV spectrum of the FITC labeled TRAIL and NM modified with FITC labeled TRAIL. (**G**) SDS-PAGE analysis was used to investigate the neutrophil membrane coated onto nanoparticles from (1) neutrophils, (2) NM and (3) NM-PN. (**H**) In vitro serum stability evaluation of NM-PN and TNM-PN in DMEM containing 10% FBS. (**I**) In vitro kinetics of the release of PTX from PN, NM-PN and TNM-PN in PBS (pH = 7.2) within 120 h.

against SKOV3 cells in comparison with T-NM, NM-PN and TRAIL+NM-PN, but the growth inhibition in NM-PN group was indistinguishable from that in TRAIL+NM-PN. The severer cytotoxicity towards SKOV3 cells induced by TNM-PN than TRAIL+NM-PN attributed to TRAIL-receptor mediated endocytosis of nanoparticles, which led to a higher rate of apoptosis. TNM-PN displayed a significant late apoptosis rate of 55.1% in annexin V/PI staining assays (Figure 3B and C), which was constant with the results of CCK-8 assay. All these results predicted the excellent potential of TNM-PN to induce tumor cell apoptosis in vivo.

To validate the enhanced cellular internalization ability of TRAIL onto TNM-PN, the DiD-labeled biomimetic nanoparticles were employed to be co-incubated with SKOV3 cells for 4 h. The fluorescence signals were further detected by CLSM and analyzed by FCM. As shown in Figure 4A, SKOV3 cells treated with TNM-PN exhibited stronger fluorescence signals than those with NM-PN, which confirmed the successful delivery of drugs and verified the compelling cellular internalization ability of TRAIL modification. The cell uptake of the TNM-PN was further quantitatively confirmed by FCM. The mean fluorescence intensity (MFI) of TNM-PN was nearly 3 times higher than that of NM-PN (Figure 4B), which was in line with the phenomena observed by CLSM. The results elucidated that the augmented cellular

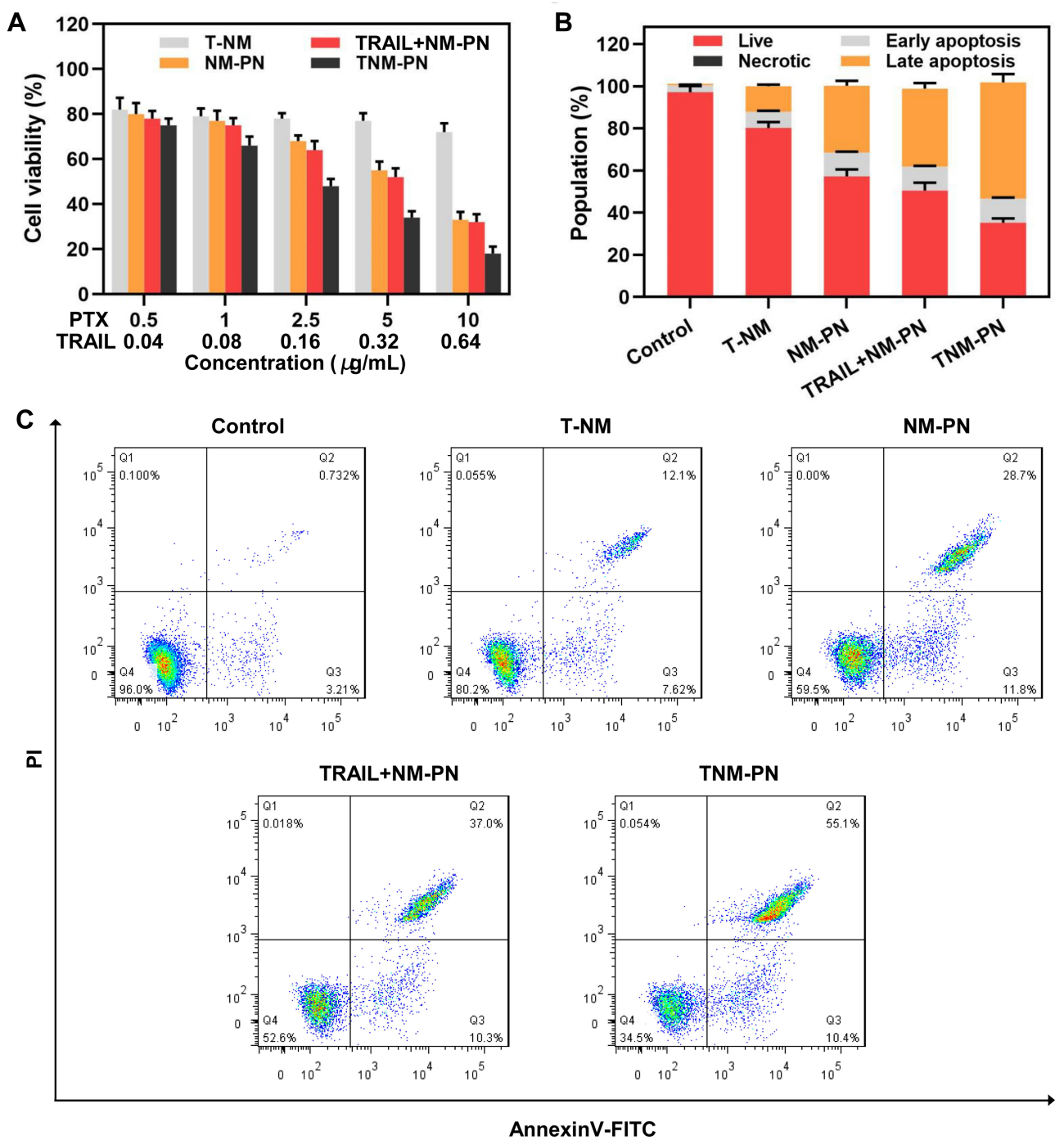

Figure 3 In vitro cytotoxicity of biomimetic nanoparticles. (**A**) In vitro cytotoxicity of SKOV3 cells treated with T-NM, NM-PN, TRAIL+NM-PN and TNM-PN for 24 h at various concentrations. (**B**) Summary data of apoptosis rate and (**C**) representative scatter plots of apoptosis of SKOV3 cells was determined by FCM following various treatments (5 μg/mL PTX and 0.32 μg/mL TRAIL equivalent) for 24 h. Data was given as the mean ± SD (n = 5).

internalization of TNM-PN was mediated via a TRAIL receptor-targeted pattern.

The capacity of immune evasion was the main enchanting feature of the cell membrane camouflaging delivery system to improve the half-life of drugs. PN, NM-PN and TNM-PN were pre-labeled with DiD for the evaluations of resistance to elimination by the reticuloendothelial system (RES). RAW 264.7 macrophages were employed as the model to simulate the resistance of neutrophil membrane camouflaging nanoparticles to immune clearance in vitro. RAW 264.7 cells were cultured with various samples for 4 h and subsequently harvested to CLSM observation. Slightest fluorescent signals

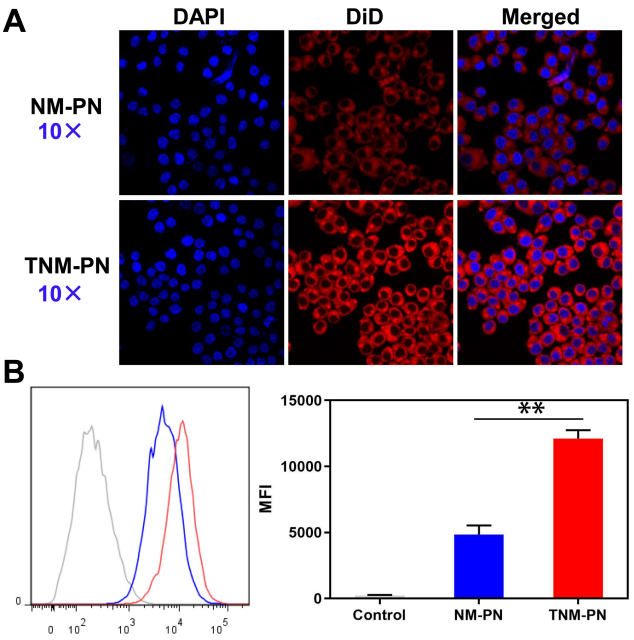

Figure 4 In vitro tumor cell uptake of biomimetic nanoparticles. (**A**) Representative confocal microscopy images of SKOV3 cells treated with NM-PN and TNM-PN for 4 h. (**B**) Quantitative analysis by FCM (left) and statistical analysis (right). Data are given as the mean ± SD (n = 3). Statistical significance was calculated via two-tailed Student's *t*-test, P-value: **p < 0.01.

were detected for TNM-PN and NM-PN group, while the fluorescent intensity was significantly improved for PN group (Figure 5A). The mean fluorescence intensities of RAW264.7 in PN, NM-PN and TNM-PN group determined by FCM were in good accordance with that of CLSM (Figure 5B). The discrepancy of neutrophil membrane camouflaging nanoparticles and PN showed that macrophages had favorable phagocytosis to heterologous substance, which implied that TNM-PN could resist to elimination by the RES due to inheriting from the traits of source cells.

DiD-labeled TNM-PN, NM-PN and PN were intravenously injected into nude mice to evaluate the blood circulation of TNM-PN, NM-PN and PN. The peripheral blood of mice was collected to obtain serum and monocytes at designated time points. As shown in Figure 5C, the fluorescence signals of serum in both TNM-PN and NM-PN groups were detectable up to 48h, while the fluorescence signals in PN group was nearly invisible after 4–12 h. The mechanism of immune elimination was investigated by detecting fluorescence signal of monocyte from peripheral blood at 4 h post-injection. The extended circulating time of TNM-PN and NM-PN group should be ascribed to neutrophil membranes coated to the biomimetic nanoparticles. Intriguingly, hardly was there any significant variance between TNM-PN and NM-PN in the blood circulation within 48 h, suggesting the blood circulation might not be influenced by the decoration of TRAIL. The isolated monocytes were purified and stained with CD11b antibody, a maker expressed universally on mononuclear phagocytes, to analyze using flow cytometry. $CD11b^+$ monocytes in the PN group displayed a significant positive fluorescence rate of 8.64%, while 1.77% and 2.35% DiD^+CD11b^+ monocytes were detected in NM-PN and TNM-PN group, respectively (Figure 5D). Therefore, neutrophil membrane coating endowed TNM-PN with convenience to escape immune elimination, prolong blood circulation and target tumors selectively.

To investigate the targeting properties of TNM-PN in vitro, HUVECs were stimulated by TNF-α to induce inflammation as well as to up-regulate ICAM-1, E-selectin and CD44, which were beneficial for cell targeting due to the specific adhesion of neutrophil membranes and HUVECs. The inflamed HUVECS were treated with DiD-labeled TNM-PN for 4 h and observed by CLSM to detect the binding behavior of TNM-PN to HUVECs. As shown in Figure 6A, HUVECs activated by TNF-α exhibited comparatively stronger red fluorescence signals of DiD-labeled TNM-PN, while negligible fluorescence signals were visualized in the HUVECs without TNF-α treatment. DiD-labeled TNM-PN were distributed on the cell membrane of inflamed HUVECs, which attributed to the upregulation of associated adhesion molecules to reinforce cell-cell interactions. The inflamed HUVECs incubated with TNM-PN were collected to quantitatively analyze the binding efficiency using FCM. The MFI in the inflamed HUVES group showed around 2.5-fold higher than that without pre-incubation with TNF-α, which was consistent with the phenomenon observed by CLSM (Figure 6B). These results indicated that TNM-PN retaining the membrane proteins of the source cells preferred sticking to inflamed endothelial cells, which was essential for subsequently targeting tumor tissues.

The in vivo biodistribution of TNM-PN was performed to analyze tumor targetability using in vivo imaging system. SKOV3 tumor-bearing nude mice were established and administrated intravenously with Ce6 preloaded TNM-PN, NM-PN and PN to imaging at 4 h, 12 h, 24 h and 48 h. As shown in Figure 7A, the TNM-PN and NM-PN tended to accumulate into the tumor site rapidly after 4 h administration, as verified by the significantly increased fluorescence signal of Ce6. The distribution profiles in major organs as well as tumors were quantitatively

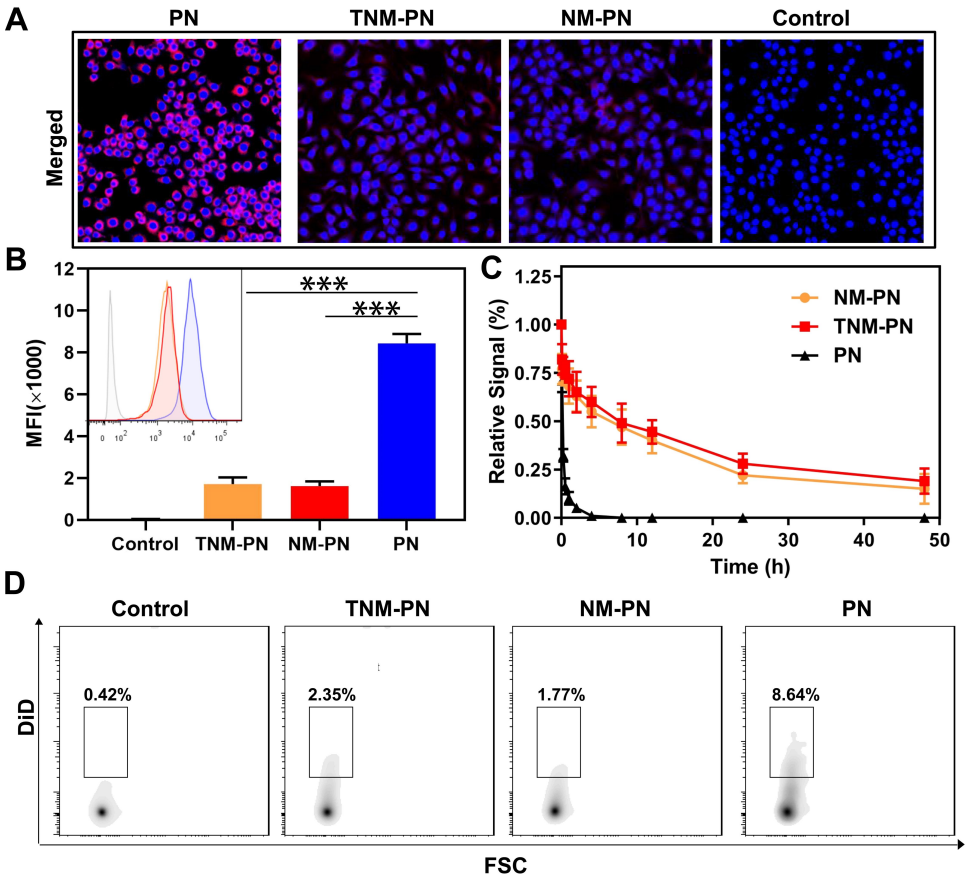

Figure 5 The immune evasion of biomimetic nanoparticles in vitro and in vivo. RAW264.7 macrophages treated with PN, TNM-PN and NM-PN with equivalent dose of DiD after co-incubation for 4 h. (**A**) Cells were observed by CLSM and (**B**) the detected by FCM with the statistical data quantified by mean fluorescence intensity. Scale bar: 25 μm. Nude mice were intravenously injected with biomimetic nanoparticles. (**C**) In vivo circulation analysis of PN, NM-PN and TNM-PN within 48 h. (**D**) Representative scatter plots images of monocytes ($CD11b^+$) uptake of control, PN, NM-PN and TNM-PN administrated for 4 h by flow cytometry. Data are given as the mean ± SD (n = 3). Statistical significance was calculated *via* two-tailed Student's *t*-test, P value: ***p < 0.001.

determined at 12 h post-injection. The fluorescence intensities at tumor site in TNM-PN and NM-PN group were notably higher than that in mice of PN group, while PN displayed more accumulation in the liver (Figure 7A–C), indicating that neutrophil membrane coating was available for highly efficient in vivo tumor-targeting delivery, and decreased the clearance by the RES. Moreover, the fluorescence was undetectable at the tumor site after 12 h for the PN, while the TNM-PN and NM-PN treated group showed a prolonged signal even after 48 h (Figure 7A–C). These results indicated that neutrophil membrane coated PLGA nanoparticles improved the biomimetic nanoparticles' circulation time in blood effectively to tumor targeting. The ex vivo biodistribution analysis of major organs showed that tumor tissues in TNM-PN group exhibited higher fluorescence intensity in comparison with the PN group, which further confirmed the higher accumulation of TNM-PN and NM-PN at tumor sites due to immune evasion (Figure 7B). The average fluorescence intensity of isolated tumor tissues in TNM-PN group exhibited almost 2-fold higher than that of NM-PN and 3-fold higher than that of PN (Figure 7C), which was mainly attributed to TRAIL modification on cell membranes by receptor-mediated endocytosis as well as the adhesive interactions between neutrophil and inflamed tumor vascular endothelial cells.

To evaluate the antitumor effect of biomimetic nanoparticles, nude mice bearing SKOV3 tumors with a volume of about 100−150 mm^3 were randomly separated into five groups PN, NM-PN, TRAIL+NM-PN and TNM-PN. The mice were intravenously injected with corresponding drugs every other day for seven times. The tumor growths of the mice in PN, NM-PN, TRAIL+NM-PN and TNM-PN group were significantly inhibited in comparison with PBS group (Figure 8A). However, the tumor volume of the mice in PN group still increased considerably on day 16, which suggested the tumor growth could not be controlled efficiently only by the passive targeting. The tumor volume in NM-PN group experienced

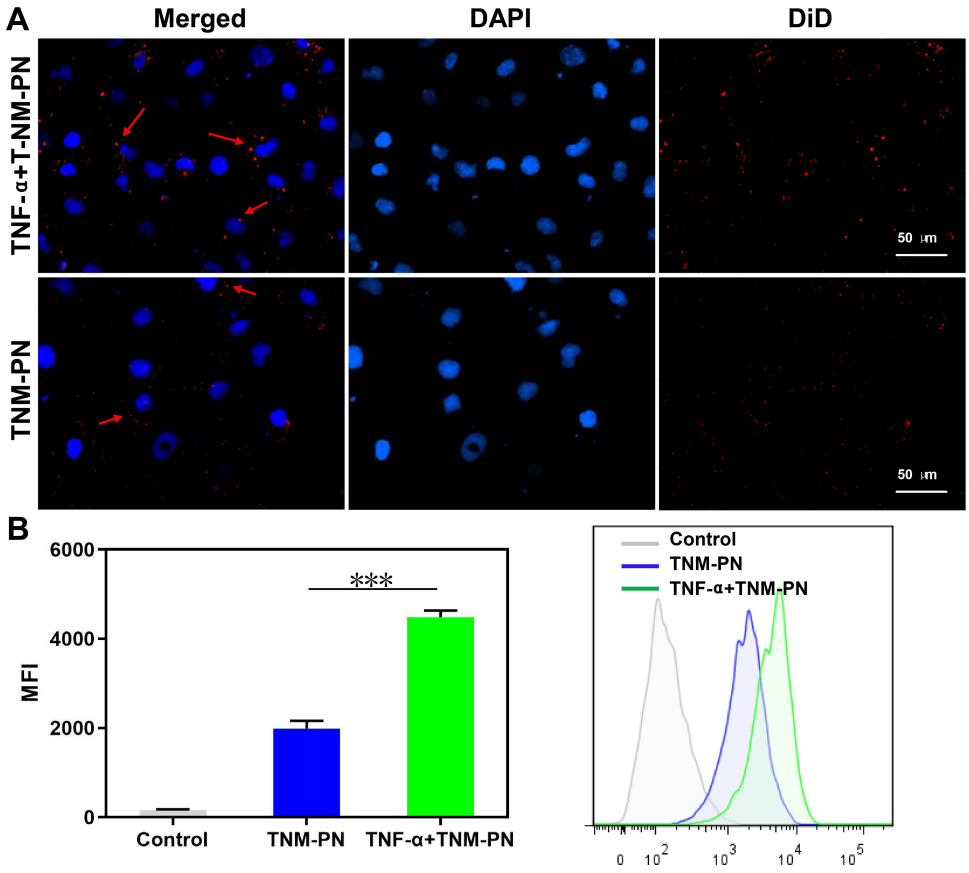

Figure 6 In vitro analysis of binding to inflamed endothelial cells. (**A**) The fluorescence images of HUVEC endothelial cells pre-treated with TNF-α and then incubated with DiD-labeled TNM-PN and observed by CLSM. (**B**) The binding efficiency quantitatively measured by FCM. The histogram of mean fluorescence intensity and representative images of flow cytometry analysis. Data are given as the mean ± SD (n = 3). Statistical significance was calculated *via* two-tailed Student's *t*-test, P-value: ***p < 0.001.

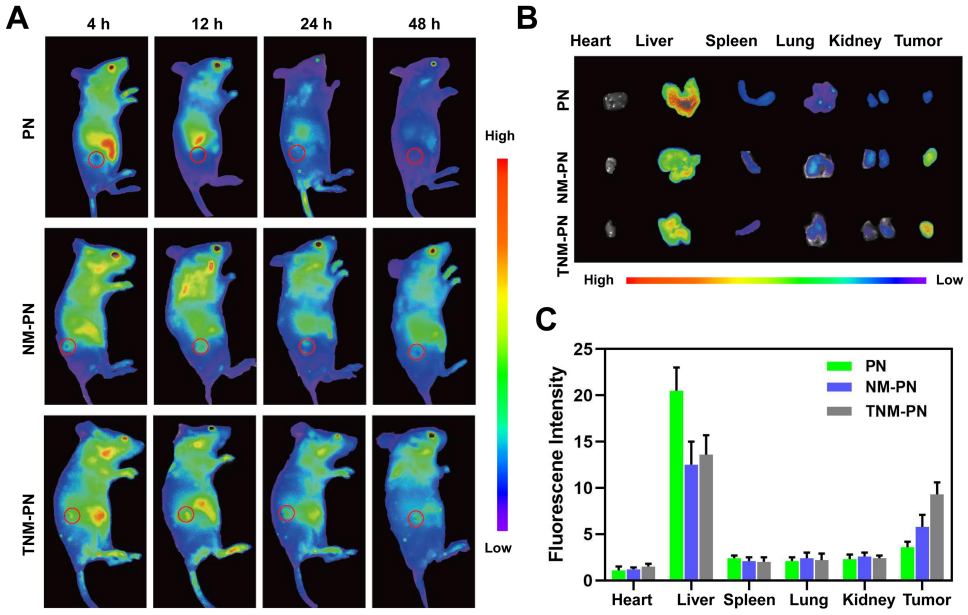

Figure 7 In vivo biodistributions of biomimetic nanoparticles in the tumor-bearing mice. (**A**) In vivo imaging of tumor-bearing nude mice at 4 h, 12 h, 24 h and 48 h after administration with Ce6 encapsulated PN, NM-PN and TNM-PN. (**B**) Ex vivo fluorescence images of major organs excised from sacrificed mice after 12 h post-injection and (**C**) fluorescence intensities of ROI analysis. Data were given as the mean ± SD (n = 3).

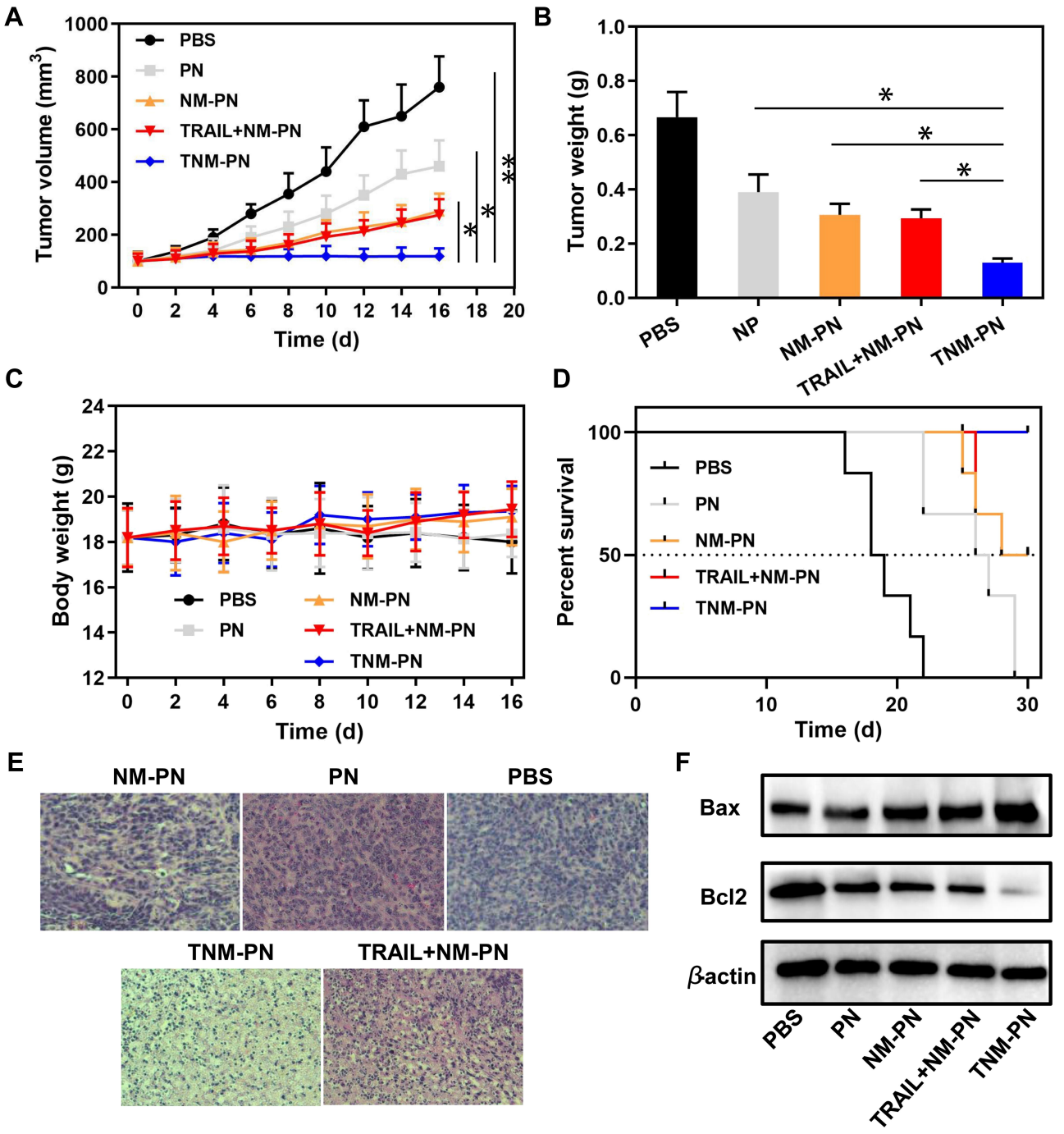

Figure 8 In vivo antitumor effect in the SKOV3 model. (**A**) Time-dependent tumor average growth curves after different treatments within 16 days. (**B**) The tumors isolated to weigh on day 16. (**C**) The body weight curves of tumor-bearing mice. (**D**) Survival rates of mice after various treatments (n = 6). (**E**) H&E staining of tumors and (**F**) tumor cell apoptosis detection by western-blot. Data were given as the mean ± SD (n = 6). Statistical significance was calculated *via* two-tailed Student's *t*-test, P-value: *p < 0.05; **p < 0.01.

moderate growth in comparison with PN group, indicative of the improved therapeutic outcome due to the adhesive interactions between neutrophils and inflamed tumor endothelial cells. Remarkably, mice in TNM-PN group showed the most retarded tumor growth at the investigated period, which was ascribed to TRAIL-mediated active targeting of tumor cells for enhanced internalization to induce apoptosis. After the mice being sacrificed, the SKOV3 tumors were isolated to weigh. The weights of the tumor further verified the excellent anti-tumor efficacy of TNM-PN (Figure 8B). H&E staining analysis of tumor slices was explored to confirm the aforementioned results.

More apoptosis or necrosis cells without nuclei were visualized in the tumor tissue of TNM-PN and NM-PN groups, while a wealth of tumor cells remained intact in the tumor tissues of both PBS and PN groups (Figure 8E). Besides, tumor cell apoptosis was further investigated by western-bot and the results showed that TNM-PN group had the most pro-apoptotic protein Bax and the least anti-apoptotic protein Bcl2 which were consistent with H&E staining analysis (Figure 8F). During this period, the body weights of the mice were also monitored, which exhibited slight changes due to the negligible systemic toxicity (Figure 8C). Besides, the survival rate in TNM-PN group remained much higher (100%) than those of other groups with a mean survival time of fewer than 30 days (Figure 8D).

Conclusions

In summary, we established a TNM-PN system that can adhere to the inflamed tumor vascular endothelial cells to boost TRAIL-mediated cellular internalization subsequently for amplifying the antitumor effect. TNM-PN was endowed with the capacity of preferring for cellular internalization, which was responsible for inducing stronger in vitro cytotoxicity and apoptosis. The tests of in vitro binding and in vivo imaging verified the compelling performance of active tumor-targeting for neutrophil membrane camouflaging and TRIAL modification on TNM-PN. Mice in TNM-PN group showed significant retarded tumor growth and the highest survival rate at the investigated period, which was ascribed to prolonged blood circulation and enhanced accumulation in the tumor. Moreover, in comparison with the prevalence of employing various cell membranes to camouflage the drug delivery system, we emphasized on the promotion of cellular internalization utilizing biomacromolecules for engineering cell membrane-based nanotherapeutics. This strategy is highly versatile and provides insights into tailoring camouflaging nanoparticles for the improvement of drug delivery.

Acknowledgments

This work was supported by the National Natural Science Foundation of China (NO. 81903172, NO. 81771560, NO. 81771560).

Disclosure

The authors declare no competing interest.

References

1. Rosenblum D, Joshi N, Tao W, Karp JM, Peer D. Progress and challenges towards targeted delivery of cancer therapeutics. *Nat Commun*. 2018;9.
2. Jin Q, Deng YY, Chen XH, Ji J. Rational design of cancer nanomedicine for simultaneous stealth surface and enhanced cellular uptake. *ACS Nano*. 2019;13(2):954–977. doi:10.1021/acsnano.8b07746
3. van der Meel R, Sulheim E, Shi Y, Kiessling F, Mulder WJM, Lammers T. Smart cancer nanomedicine. *Nat Nanotechnol*. 2019;14(11):1007–1017. doi:10.1038/s41565-019-0567-y
4. Sun QH, Zhou ZX, Qiu NS, Shen YQ. Rational design of cancer nanomedicine: nanoproperty integration and synchronization. *Adv Mater*. 2017;29.
5. Yang JL, Wang F, Lu Y, et al. Recent advance of erythrocyte-mimicking nanovehicles: from bench to bedside. *J Control Release*. 2019;314:81–91. doi:10.1016/j.jconrel.2019.10.032
6. Fang RH, Kroll AV, Gao WW, Zhang LF. Cell membrane coating nanotechnology. *Adv Mater*. 2018;30.
7. Wang HJ, Wang K, He LH, Liu YQ, Dong HQ, Li YY. Engineering antigen as photosensitiser nanocarrier to facilitate ROS triggered immune cascade for photodynamic immunotherapy. *Biomaterials*. 2020;244:119964. doi:10.1016/j.biomaterials.2020.119964
8. Wårdell K. 46th ESAO congress 3–7 september 2019 Hannover, Germany abstracts. *Int J Artif Organs*. 2019;42(8):386–474. doi:10.1177/0391398819860985
9. Li JC, Zhen X, Lyu Y, Jiang YY, Huang JG, Pu KY. Cell membrane coated semiconducting polymer nanoparticles for enhanced multimodal cancer phototheranostics. *ACS Nano*. 2018;12(8):8520–8530. doi:10.1021/acsnano.8b04066
10. Rao L, Bu LL, Xu JH, et al. Red blood cell membrane as a biomimetic nanocoating for prolonged circulation time and reduced accelerated blood clearance. *Small*. 2015;11(46):6225–6236. doi:10.1002/smll.201502388
11. Zhen X, Cheng PH, Pu KY. Recent advances in cell membrane-camouflaged nanoparticles for cancer phototherapy. *Small*. 2019;15(1):15. doi:10.1002/smll.201804105
12. Wang HJ, Liu Y, He RQ, Xu DL, Zang J, Weeranoppanant N. Cell membrane biomimetic nanoparticles for inflammation and cancer targeting in drug delivery. *Biomater Sci*. 2020;8(2):552–568. doi:10.1039/C9BM01392J
13. Muller WA. Getting leukocytes to the site of inflammation. *Vet Pathol*. 2013;50(1):7–22. doi:10.1177/0300985812469883
14. Dong XY, Gao J, Zhang CY, Hayworth C, Frank M, Wang ZJ. Neutrophil membrane-derived nanovesicles alleviate inflammation to protect mouse brain injury from ischemic stroke. *ACS Nano*. 2019;13(2):1272–1283. doi:10.1021/acsnano.8b06572
15. Palomba R, Parodi A, Evangelopoulos M, et al. Biomimetic carriers mimicking leukocyte plasma membrane to increase tumor vasculature permeability. *Sci Rep*. 2016;6.
16. Zhang C, Zhang L, Wu W, et al. Artificial super neutrophils for inflammation targeting and HClO generation against tumors and infections. *Adv Mater*. 2019;31.
17. Kang T, Zhu QQ, Wei D, et al. Nanoparticles coated with neutrophil membranes can effectively treat cancer metastasis. *ACS Nano*. 2017;11(2):1397–1411. doi:10.1021/acsnano.6b06477
18. Blanco E, Shen H, Ferrari M. Principles of nanoparticle design for overcoming biological barriers to drug delivery. *Nat Biotechnol*. 2015;33:941–951. doi:10.1038/nbt.3330
19. Johnstone RW, Frew AJ, Smyth MJ. The TRAIL apoptotic pathway in cancer onset, progression and therapy. *Nat Rev Cancer*. 2008;8(10):782–798. doi:10.1038/nrc2465
20. Dai XY, Zhang JW, Arfuso F, et al. Targeting TNF-related apoptosis-inducing ligand (TRAIL) receptor by natural products as a potential therapeutic approach for cancer therapy. *Exp Biol Med*. 2015;240(6):760–773. doi:10.1177/1535370215579167

21. Guimaraes PPG, Gaglione S, Sewastianik T, Carrasco RD, Langer R, Mitchell MJ. Nanoparticles for immune cytokine TRAIL-based cancer therapy. *ACS Nano*. 2018;12(2):912–931. doi:10.1021/acsnano.7b05876
22. Pan LQ, Wang HB, Xie ZM, et al. Novel conjugation of tumor-necrosis-factor-related apoptosis-inducing ligand (TRAIL) with monomethyl auristatin e for efficient antitumor drug delivery. *Adv Mater*. 2013;25(34):4718–4722. doi:10.1002/adma.201301385
23. Fulda S. Safety and tolerability of TRAIL receptor agonists in cancer treatment. *Eur J Clin Pharmacol*. 2015;71(5):525–527. doi:10.1007/s00228-015-1823-1
24. Dianat-Moghadam H, Heidarifard M, Mahari A, et al. TRAIL in oncology: from recombinant TRAIL to nano- and self-targeted TRAIL-based therapies. *Pharmacol Res*. 2020;155:155. doi:10.1016/j.phrs.2020.104716
25. Wong SHM, Kong WY, Fang CM, et al. The TRAIL to cancer therapy: hindrances and potential solutions. *Crit Rev Oncol Hematol*. 2019;143:81–94. doi:10.1016/j.critrevonc.2019.08.008
26. Zhong HH, Wang HY, Li J, Huang YZ. TRAIL-based gene delivery and therapeutic strategies. *Acta Pharmacol Sin*. 2019;40(11):1373–1385. doi:10.1038/s41401-019-0287-8
27. Belkahla H, Herlem G, Picaud F, et al. TRAIL-NP hybrids for cancer therapy: a review. *Nanoscale*. 2017;9(18):5755–5768. doi:10.1039/C7NR01469D
28. Xue JW, Zhao ZK, Zhang L, et al. Neutrophil-mediated anticancer drug delivery for suppression of postoperative malignant glioma recurrence. *Nat Nanotechnol*. 2017;12(7):692–700. doi:10.1038/nnano.2017.54
29. Bae S, Ma K, Kim TH, et al. Doxorubicin-loaded human serum albumin nanoparticles surface-modified with TNF-related apoptosis-inducing ligand and transferrin for targeting multiple tumor types. *Biomaterials*. 2012;33(5):1536–1546. doi:10.1016/j.biomaterials.2011.10.050
30. Jiang TY, Mo R, Bellotti A, Zhou JP, Gu Z. Gel-liposome-mediated co-delivery of anticancer membrane-associated proteins and small-molecule drugs for enhanced therapeutic efficacy. *Adv Funct Mater*. 2014;24(16):2295–2304. doi:10.1002/adfm.201303222
31. Danhier F, Ansorena E, Silva JM, Coco R, Le Breton A, Preat V. PLGA-based nanoparticles: an overview of biomedical applications. *J Control Release*. 2012;161(2):505–522. doi:10.1016/j.jconrel.2012.01.043
32. Wu MY, Zhang HX, Tie CJ, et al. MR imaging tracking of inflammation-activatable engineered neutrophils for targeted therapy of surgically treated glioma. *Nat Commun*. 2018;9(1). doi:10.1038/s41467-018-07250-6.